A Second-order Finite Difference Scheme For The Wave Equation on a Reduced Polar Grid

Abstract. This paper presents a second-order numerical scheme, based on finite differences, for solving the wave equation in polar and cylindrical domains. This method is defined on a reduced polar grid with nodes that are a subset of a uniform polar grid and are chosen so that the distance between nodes is near constant. This method is capable of computing the wave equation at a fraction of the computational cost of common second-order finite difference schemes defined on uniform polar grids but still maintains a comparable level of accuracy.

B. Holman

Department of Mathematics, University of Arizona, Tucson, AZ 85721, USA

E-mail: bholman@math.arizona.edu

L. Kunyansky

Department of Mathematics, University of Arizona, Tucson, AZ 85721, USA

Keywords: wave equation, polar grid, uniform polar grid, reduced polar grid, finite difference, second-order finite difference

1. Introduction

We solve the wave equation in polar and cylindrical domains using a finite difference numerical scheme. The wave equation is widely used in fields such as acoustics, biomedical imaging, fluid mechanics, radar/sonar, and electromagnetics. Our immediate motivation for this research comes from thermo-acoustic (and photo-acoustic) tomography where image reconstruction can be performed using the method of time reversal [15, 8] which requires a numerical method for computing the solution to the wave equation with Dirichlet boundary conditions. With this application in mind there are two important factors to consider. First, tomographic data has a high level of error and reconstructions can posses discontinuities; thus, higher-order numerical schemes based on polynomial interpolation offer no advantage. Second, many tomographic applications require high resolution reconstructions which entails the use of large spatial grids.

A naïve approach for solving the wave equation in polar domains is to use a spatial grid with uniform angular and radial spacing and finite difference stencils to compute derivatives. However, a consequence of having a uniform angular spacing between grid nodes is that nodes are clustered near the origin; the distance between nodes on the inner-most annulus is $2\Delta r \sin(\frac{\Delta\theta}{2})$, where Δr and $\Delta\theta$ are the radial and

angular spacing respectively. This has adverse effects on the stability of the scheme. Recall that the stability of finite difference schemes on Cartesian grids depends on a ratio between the temporal step size and the distance between nodes; a similar ratio has been observed numerically for polar grids. Despite the significant body of research regarding finite difference schemes on non-uniform Cartesian grids [2, 10], there are few results on finite difference schemes for non-uniform polar grids in the literature. Some methods for finite difference schemes in cylindrical coordinates allow for the 'stretching' of grids [3, 11] but to the knowledge of the author, no finite difference schemes have yet been produced that allow for the removal of nodes from a uniform polar grid. Other researches have attempted to numerically solve the wave equation in polar domains by simply interpolating boundary conditions defined on circles onto Cartesian grids [4] or more generally by using an embedded boundary to immerse a Cartesian grid inside a boundary[6, 5]; but, although the method presented in [5] is second-order accurate, it requires the addition of small artificial terms to the Dirichlet boundary data and a fourth-order dissipative term for stability.

Researchers in the meteorology community frequently deal with Gaussian grids defined on the surface of a sphere and as such have encountered problems dealing with the clustering of grid nodes. One method they developed uses finite differences on uniform Gaussian grids with a large temporal step size but requires filtering high frequency modes at each time step; a process that increases computational time and decreases accuracy [13]. Spectral methods defined on 'reduced' Gaussian grids have also been introduced [7, 14] but this approach does not offer advantages in our applications.

Here, we present a finite difference numerical scheme that permits time steps which are significantly larger then those allowed by traditional finite difference schemes on uniform polar grids. This is achieved by eliminating the clustering of nodes near the origin.

The reduced polar grid is described in section 2.2. The finite difference stencils and interpolation techniques used by this method are provided in section 2.3 and are rigorously proven to be second-order accurate. Section 3 provides numerical evidence that this scheme is stable and uses the two-dimensional algorithm defined on a disk to compute the solution to the wave equation in a three-dimensional cylinder. Lastly, section 4 illustrates the efficiency of the present method in comparison to finite difference schemes on a uniform polar grid.

2. Numerical scheme

We consider a numerical scheme for computing the solution to the following initial value/boundary value partial differential equation:

$$\begin{cases} \frac{\partial^2}{\partial t^2}u = \Delta u & (r,\theta,t) \in \Omega \times [0,T] \\ u(R,\theta,t) = g(\theta,t) \\ u(r,\theta,0) = f(r,\theta) \\ \frac{\partial}{\partial t}u(r,\theta,0) = 0, \end{cases} \tag{1}$$

where Ω is the a disk with radius R, T is a finite amount of simulation time, and $g(\theta, t)$ is boundary data. Our approach is to discretize the spatial domain by a grid that is a subset of a uniform polar grid. Spatial derivatives are computed using three different finite difference stencils and a pseudo-spectral method.

2.1. Temporal discretization

We compute the solution of problem (1) at discrete time steps according to the following difference equation:

$$u^{n+1} = 2u^n - u^{n-1} + \Delta t^2 \Delta u^n.$$

This time stepping in combination with the spatial discretization (described in detail later) produces a method for simulating the wave equation that is second-order accurate. First, we present a spatial grid on which u is defined for each discrete time step. Then, we present a method to numerically approximate the Laplacian of a function defined on the numerical grid to second-order accuracy.

2.2. Spatial grid

A uniform polar grid is a grid where the radial spacing, Δr, and angular spacing, $\Delta\theta$, between grid nodes is held constant. Our approach is to perform computations on a subset of a uniform polar grid which eliminates the clustering of nodes near the origin. We introduce a *reduced polar grid* with nodes chosen so that the density of grid nodes is near constant.

For notation, let the annuli of grid nodes be numbered starting in the center so that the inner-most annulus, where $r = \Delta r$, is denoted A_1 and in general A_k is an annulus of radius $r = k\Delta r$. A_1 is chosen to have L equispaced nodes with a node at the point $(\Delta r, 0)$. The number of nodes on annulus A_k is $L \cdot 2^{n-1}$ where n is the integer such that $2^{n-1} \leq k < 2^n$. Additionally, we require that each annulus have a point at the angle $\theta = 0$. The resulting reduced polar grid has regions where the angular spacing between nodes is constant and is depicted in figure 2. A result of varying the number of nodes on each annulus in the manner described is that the arclength between two adjacent nodes on the same annulus is uniformly bounded from both above and below in terms of Δr,

$$\frac{2\pi}{L}\Delta r \leq \Delta\theta r < \frac{4\pi}{L}\Delta r. \tag{2}$$

There are logarithmically many adjacent annuli that have different angular spacing between nodes; two such annuli are referred to as *transition layers*.

2.3. Approximation of spatial derivatives

In order to compute the solution to equation (1) using the time stepping described in section 2.1 the Laplacian must be computed at each iterate. Our scheme uses centered finite difference stencils to approximate the Laplacian at most nodes of the spatial grid.

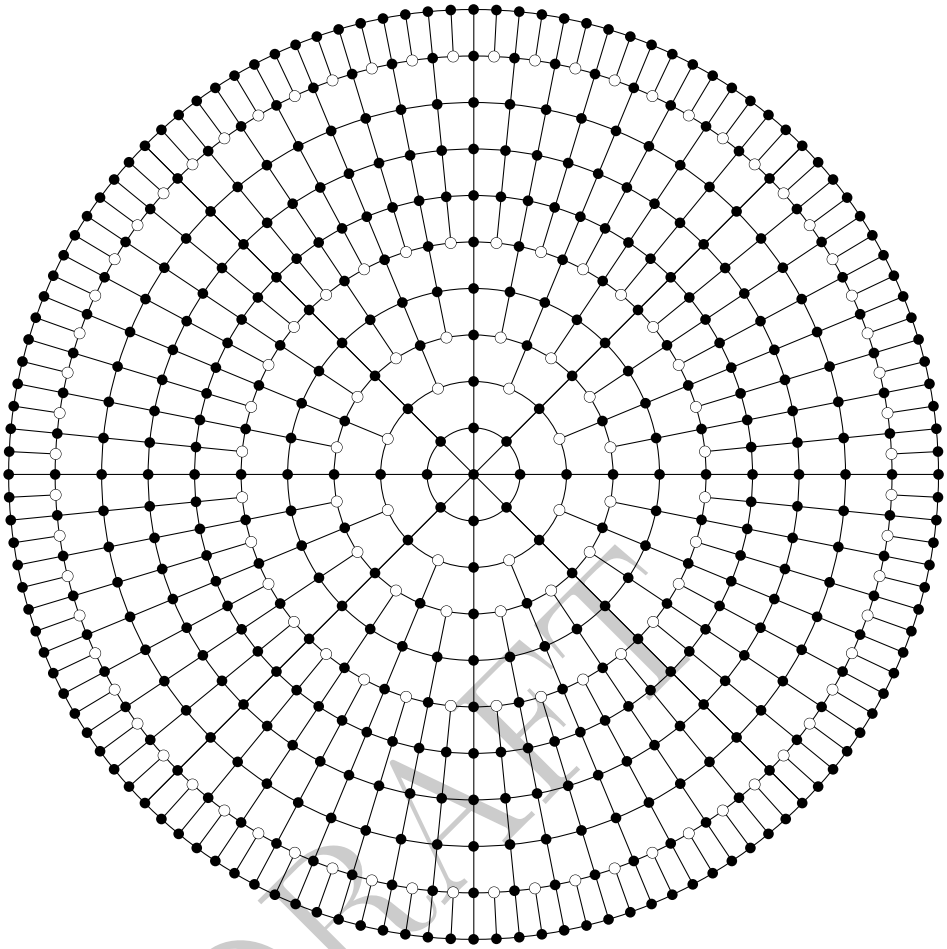

Figure 1. Depiction of the first 10 annuli of the polar grid.

These stencils are not well defined at half of the nodes contained within a transition layer; the Laplacian is interpolated at these points. Additionally, near the center of the grid algorithm 2.0.1 is used to approximated angular derivatives.

The numerical method presented here is a second-order accurate numerical scheme; higher-order schemes can be constructed in much the same manner as this one. The spatial grid is divided into two regions according to a parameter η; we fixed $\eta = 0.1$ but any fixed constant will result in a second-order method. The first region contains grid nodes where spatial derivatives are computed according to 2.3.1 and are determined by $r > \eta R$. The second region contains grid nodes where spatial derivatives are computed according to 2.3.2 and are determined by $r \leq \eta R$.

2.3.1. Outer region, $r > \eta R$ Recall that the Laplacian in polar coordinates is,

$$\Delta u = \frac{\partial^2}{\partial r^2} u + \frac{1}{r} \frac{\partial}{\partial r} u + \frac{1}{r^2} \frac{\partial^2}{\partial \theta^2} u.$$

In this region of the spatial grid radial derivatives are approximated by the second-order centred finite difference stencils

$$\frac{\partial}{\partial r}u_{i,j} \approx \frac{u_{i+1,j} - u_{i-1,j}}{2\Delta r}, \qquad |\mathcal{E}_{rr}| \leq \frac{\Delta r^2}{6}M$$

and

$$\frac{\partial^2}{\partial r^2}u_{i,j} \approx \frac{u_{i+1,j} - 2u_{i,j} + u_{i-1,j}}{\Delta r^2}, \qquad |\mathcal{E}_{rr}| \leq \frac{\Delta r^2}{6}M,$$

where $\mathcal{E}_{rr}$ is the error term associated with these stencils and M is a uniform bound on the third derivative of u for any $(r, \theta) \in \Omega$ and $r > \eta R$,

$$\max\left\{\left|\frac{\partial^3}{\partial r^3}u(r,\theta)\right|, \left|\frac{\partial^3}{\partial \theta^3}u(r,\theta)\right|\right\} \leq M < \infty.$$

The angular stencil is

$$\frac{\partial^2}{\partial \theta^2}u_{i,j} \approx \frac{u_{i,j+1} - 2u_{i,j} + u_{i,j-1}}{\Delta \theta^2}, \qquad |\mathcal{E}_{\theta\theta}| \leq \frac{\Delta \theta^2}{6}M.$$

Inequality (2) can be used to bound $\Delta\theta$ of $\mathcal{E}_{\theta\theta}$ in terms of Δr,

$$|\mathcal{E}_{\theta\theta}| \leq \frac{\Delta\theta^2}{6}M < \frac{(4\pi\Delta r)^2}{6L^2r^2}M.$$

Now, the error associated with using the specified finite difference stencils to approximate the Laplacian in polar coordinates in the outer region of the numeric grid can be bounded as a function of the radius with a coefficient of Δr^2; that is,

$$|\mathcal{E}_{outer}(r)| = \left|\mathcal{E}_{rr} + \frac{1}{r}\mathcal{E}_{rr} + \frac{1}{r^2}\mathcal{E}_{\theta\theta}\right| \leq \Delta r^2 \frac{M}{6}\left(1 + \frac{1}{r} + \frac{(4\pi)^2}{L^2r^4}\right).$$

In the outer region of the numeric grid, where r is bounded away from zero, this error decreases quadratically quickly as Δr decreases.

2.3.2. Inner region, $r \leq \eta\ R$ In this region of the spatial grid radial derivatives are approximated by the second-order centred finite difference stencils

$$\frac{\partial}{\partial r}u_{i,j} \approx \frac{-u_{i+2,j} + 8u_{i+1,j} - 8u_{i-1,j} + u_{i-2,j}}{12\Delta r}, \qquad |\mathcal{E}_r| \leq \frac{\Delta r^4}{120}K$$

and

$$\frac{\partial^2}{\partial r^2}u_{i,j} \approx \frac{u_{i+1,j} - 2u_{i,j} + u_{i-1,j}}{\Delta r^2}, \qquad |\mathcal{E}_{rr}| \leq \frac{\Delta r^2}{6}K,$$

where $\mathcal{E}_{rr}$ is as before and $\mathcal{E}_r$ is the error term associated with the new stencil for the first radial derivative. K is a uniform bound on the following derivatives of u for any $(r, \theta) \in \Omega$ and $r \leq \eta R$,

$$\max\left\{\left|\frac{\partial^5}{\partial r^5}u(r,\theta)\right|, \left|\frac{\partial^3}{\partial \theta^3}u(r,\theta)\right|\right\} \leq K < \infty.$$

In this region $\frac{\partial^2}{\partial\theta^2}u$ is computed by splitting u two parts: one that oscillates slowly with respect to θ and a second that is the remainder. The second angular derivative of the slowly oscillating part is computed spectrally, in a theoretically exact manner. The second angular derivative of the remainder of u is computed using the second-order accurate finite difference stencil of the previous section. This scheme is detailed in algorithm 2.0.1.

Algorithm 2.0.1 (Pseudo-Spectral Angular Differentiation) *Compute $\frac{\partial^2}{\partial\theta^2}u$ by differentiating the first N harmonics spectrally and all other harmonics using second-order accurate finite differences (we use $N = 3$).*

- *Let u_j ($0 \leq j < M$) be M equispaced samples of a function on annulus A_k. Decompose u_j into its first N harmonics plus higher-order frequencies. That is, for $m \leq N$ compute*

$$a_m = \frac{\Delta\theta}{\pi}\sum_{j=0}^{M-1} u_j \cos(mj\Delta\theta)$$

$$b_m = \frac{\Delta\theta}{\pi}\sum_{j=1}^{M-1} u_j \sin(mj\Delta\theta)$$

$$u_j^F = u_j - \frac{a_0}{2} - \sum_{m=1}^{N} a_m \cos(mj\Delta\theta) + b_m \sin(mj\Delta\theta)$$

- *Approximate the second derivative of the higher frequencies, u^F, by the second-order finite difference stencil given in 2.3.1. Approximate the second derivative of the lower frequencies by spectral differentiation.*

$$\frac{\partial^2}{\partial\theta^2}u_j^S = -\sum_{m=1}^{N} a_m m^2 \cos(mj\Delta\theta) + b_m m^2 \sin(mj\Delta\theta)$$

- *Add the computed derivatives of u_j^F and u_j^S to produce $\frac{\partial^2}{\partial\theta^2}u$*

Things to write:

- Error term for angular differentiation (valid near zero):
  - Compute a Taylor Series in Cartesian coordinates centred at $x = y = 0$.
  - Convert to polar coordinates.
  - Show that all terms with angular frequency larger then three have a coefficient of r to a power that is larger than three. These not only decrease in magnitude as $r \to 0$ but also are the terms not computed exactly by algorithm 2.0.1 and thus are a part of the error term for the second-order finite difference stencil.
- Determine a bound on the function $\mathcal{E}_{inner}(r)$.
- Evaluate $\mathcal{E}_{inner}(r)$ on annulus A_k and show quadratic rate of decay.

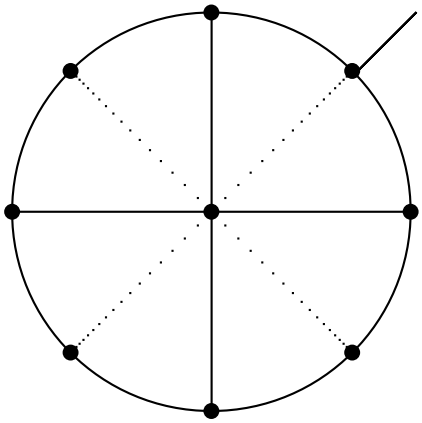

Figure 2. Depiction of stencils used at the origin. The Cartesian Laplacian is computed using both the solid lines and the dashed lines. These two approximations to the Laplacian are averaged.

2.3.3. Differentiation at the Origin The center of the polar grid is a singular point of the Laplacian in polar coordinates and there are several ways to approach differentiating through or around this singularity. Some researchers impose pole conditions at such singularities and are able to compute derivatives with high accuracy by using series expansions [1]. Other researchers avoid this singularity by using a shifted numerical grid that does not have a node at $r = 0$ [9, 12]. However, because of the spatial structure of our numerical grid, the Laplacian at the origin can be computed by simply switching to a Cartesian Coordinate system. The inner most annulus ($r = \Delta r$) has eight equispaced nodes. Thus, lines which connect nodes on the inner-most annulus to the center of the gird form two sets of mutually orthogonal lines. Figure **??** depicts these two sets of lines, one set is the union of the two solid black lines and the second is the union of the two dashed lines. Along these lines the second-order finite difference stencil can be used to approximate the Cartesian Laplacian. The two approximate values of the Laplacian obtained from the two sets of lines are averaged.

3. Numeric tests of computational method

The aforementioned differentiation scheme can be used to approximate the Laplacian at all nodes not in a transition layer and to half of the nodes in a transition layer. As mentioned previously, the Laplacian is interpolated on grid nodes where centred finite difference stencils are not defined. We tested several common interpolations schemes: spectral interpolation, cubic interpolation, and linear interpolation. All of these interpolation schemes are at least second-order accurate with respect to the angular spacing between nodes. A note should be made that although a fast spectral interpolation method requires $\mathcal{O}(n \log n)$ operations, there are logarithmically many transition layers so the time complexity of computing the Laplacian using this numerical method is still $\mathcal{O}(n^2)$. All of our numeric examples us cubic interpolating polynomials to interpolate the Laplacian onto nodes in a transition layer.

3.1. Convergence of spatial stencils

Figure 3 displays the error in computing the Laplacian of eigenfunctions of the Neumann Laplacian using the described numerical scheme. The ratios in the table indicate that the scheme is second-order accurate because doubling the number of radial points (which in-turn increases the number of angular points) in the numerical grid results in an approximation of the Laplacian that is roughly four times more accurate.

Bessel Function	Root Number	Number of Radial Points	L^2 Error	Ratio of Error
$m = 0$	$n = 5$	32	2.1247E-2	-
		64	5.2174E-3	4.072
		128	1.2920E-3	4.038
		256	3.2022E-4	4.035
		512	7.9724E-5	4.017
		1024	1.9908E-5	4.005
$m = 1$	$n = 5$	32	2.6736E-2	-
		64	1.4188E-2	1.884
		128	3.6593E-3	3.877
		256	9.1835E-4	3.985
		512	2.2939E-4	4.003
		1024	5.7281E-5	4.005
$m = 2$	$n = 5$	32	2.6096E-2	-
		64	8.2108E-3	3.178
		128	1.4583E-3	5.631
		256	3.0551E-4	4.773
		512	7.1979E-5	4.244
		1024	1.7696E-5	4.067
$m = 10$	$n = 5$	32	3.286E-2	-
		64	8.2436E-3	3.987
		128	2.0676E-3	3.987
		256	5.1766E-4	3.994
		512	1.2950E-4	3.997
		1024	3.2384E-5	3.99

Figure 3. Error in computing the Laplacian of the Eigenfunction $J_m(j'_{m,n}r)\cos(m\theta)$ (where m denotes the Bessel function and $j'_{m,n}$ is the n^{th} critical point).

3.2. Wave equation in a disk

Validation of this method is provided by integrating eigenfunctions of the Neumann Laplacian forward in time. If the wave equation with Neumann boundary conditions and zero initial temporal derivative (equation (1)) has an initial condition that is a single eigenfunction, $J_{|m|}(r\lambda_{m,n})e^{im\theta}$, then the exact solution is

$$u(r, \theta, t) = J_{|m|}(r\lambda_{m,n})e^{im\theta}\cos(\lambda_{m,n}t).$$

Bessel Function	Root Number	Number of Radial Points	L^2 Error	Ratio of Error
$m = 0$	$n = 5$	32	0.11255	-
		64	4.4872E-2	2.51
		128	1.1533E-2	3.89
		256	2.8543E-3	4.04
		512	7.0870E-4	4.03
		1024	1.7685E-4	4.01
$m = 1$	$n = 5$	32	0.1076	-
		64	2.1835E-2	4.93
		128	4.9510E-3	4.41
		256	1.2028E-3	4.12
		512	2.9787E-4	4.04
		1024	7.4180E-5	4.02
$m = 2$	$n = 5$	32	0.1036	-
		64	3.1948E-2	3.24
		128	8.8414E-3	3.62
		256	2.2710E-3	3.89
		512	5.7066E-4	3.98
		1024	1.4268-4	3.99
$m = 10$	$n = 5$	32	0.3001	-
		64	1.2371E-2	24.26
		128	1.3759E-3	8.99
		256	3.2334E-4	4.26
		512	8.0820E-5	4.00
		1024	2.020E-5	4.00

Figure 4. Error of numerical solutions to (1) with initial condition $J_m(j'_{m,n}r)\cos(m\theta)$ (where m denotes the Bessel function and $j'_{m,n}$ is the n^{th} critical point). Each simulation was integrated forward in time for 100 periods of the exact solution, $J_m(j'_{m,n}r)\cos(m\theta)\cos(tj'_{m,n})$; that is, until time $t = \frac{100}{j'_{m,n}}$.

Several eigenfunctions of the Neumann Laplacian were used as initial conditions for problem (1) and the numerical method was used to integrate each system forward in time for 100 periods of the exact solution. The Dirichlet boundary data ($g(\theta, t)$ in (1)) was computed from the exact solution. The relative L^2 error of each computed solution appears to decrease by a factor of four when the number of radial points is doubled; suggesting that the method, including spatial stencils, interpolations, and time stepping, is second-order accurate.

3.3. Wave equation in a cylinder

The two-dimensional numerical method for computing the Laplacian in a disk was used to compute the solution to the wave equation in a three-dimensional cylinder with radius

1 centred at the origin with height 1. That is, we solve the Dirichlet problem:

$$\begin{cases} \frac{\partial^2}{\partial t^2}u = \Delta u & (r,\theta,z,t) \in \Omega \times [0,T] \\ u(r,\theta,z) = g(r,\theta,t) & (r,\theta,z) \in \partial\Omega \\ u(r,\theta,z,0) = f(r,\theta,z) & \\ \frac{\partial}{\partial t}u(r,\theta,z,0) = 0, & \end{cases} \tag{3}$$

where, Ω is the cylinder and

$$\Delta u = \frac{\partial^2}{\partial r^2}u + \frac{1}{r}\frac{\partial}{\partial r}u + \frac{1}{r^2}\frac{\partial^2}{\partial \theta^2}u + \frac{\partial^2}{\partial z^2}u.$$

The cylinder is discretized into slices with width $\Delta z = \Delta r$ where each slice is a reduced polar grid. The Laplacian within the cylinder is computed using the same spatial stencils and interpolations used in section 3.2 for the r and θ variables and $\frac{\partial^2}{\partial z^2}u$ is computed using the second-order accurate finite difference stencil. Similar to the two-dimensional tests, Eigenfunctions of the Neumann Laplacian in this domain are used as initial conditions of problem (3) and the relative L^2 error after a fixed amount of time is computed. Figure 5 displays data taken from several eigenfunctions. These tests suggest that our method

Bessel Function	Root Number	$z-$Frequency	Number of Radial Points	L^2 Error	Ratio of Error
$m=0$	$n=5$	$k=5$	32	1.2490E-1	-
			64	3.0169E-2	4.14
			128	7.4473E-3	4.05
			256	1.8457E-3	4.03
$m=1$	$n=5$	$k=5$	32	1.1143E-1	-
			64	2.6447E-2	4.32
			128	6.4994E-3	4.07
			256	1.6302E-3	4.01
$m=2$	$n=5$	$k=5$	32	1.1367E-1	-
			64	2.2720E-2	4.18
			128	6.8740E-2	3.96
			256	1.7246E-3	3.99
$m=10$	$n=5$	$k=5$	32	1.687E-1	-
			64	4.0743E-2	4.14
			128	1.0128E-2	4.02
			256	2.5270E-3	4.01

Figure 5. Error of numerical simulations with initial condition $J_m(j'_{m,n}r)\cos(m\theta)\cos(zk\pi)$ (where m denotes the Bessel function and $j'_{m,n}$ is the n^{th} critical point). Each simulation was integrated forward in time for 10 periods of the exact solution, $J_m(j'_{m,n}r)\cos(m\theta)\cos(zk\pi)\cos\left(t\sqrt{j'^2_{m,n}+k^2\pi^2}\right)$; that is, until time $t = \frac{10}{\sqrt{j'^2_{m,n}+k^2\pi^2}}$.

is second-order accurate when computing the wave equation with smooth functions.

4. Comparison to uniform polar grid

The numerical scheme presented is capable of computing the wave equation significantly faster then finite differences on a uniform polar grid and still maintains a comparable level of accuracy. Figure 6 displays the computation time consumed in integrating an initial condition that is an eigenfunction of the Neumann Laplacian forward in time for one period on a log-log scale. Notice that these simulations were integrated over a time period 100 times shorter then that used in figures 3 and 4 (a consequence of the computational resources needed to integrate uniform polar grids forward in time). Figure 6 also displays the amount of computation time needed to produce each one of these solutions. The uniform polar grid has fourth-order time complexity when holding the simulation time fixed (evidenced by a slope of 3.94 on the log-log scale). Meanwhile, the numerical method on a reduced grid has a time complexity of 2.52, resulting in significantly faster computation times.

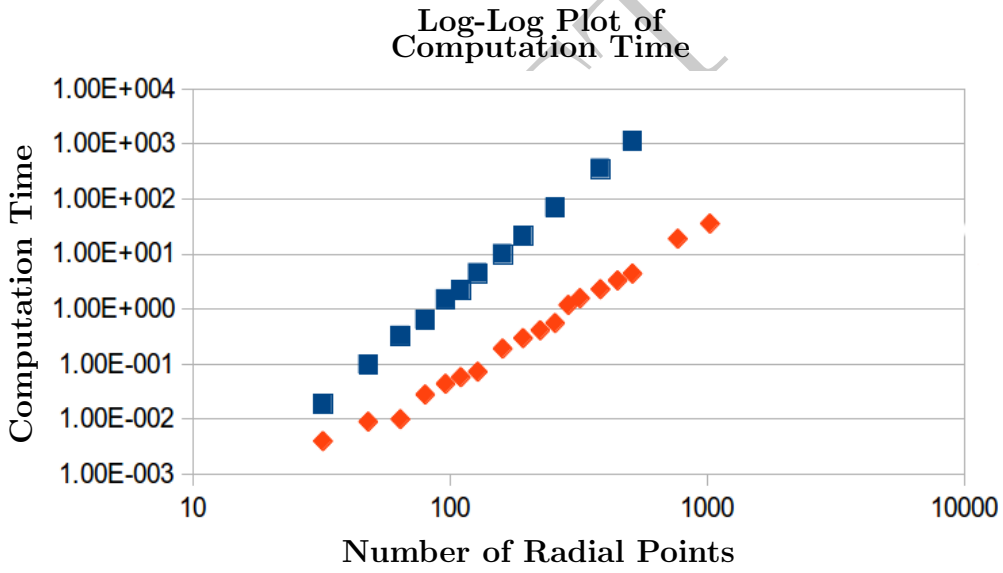

Figure 6. Log-Log plot of the computation time to integrate $J_2(j'_{2,2}r)\cos(2\theta)$ forward in time one period of the exact solution. The slope of the line fitted to the uniform grid data is 3.94 and the slope of the line fitted to the non-standard grid is 2.52.

5. Conclusion

This paper presented an efficient second-order accurate numerical method for computing the wave equation in polar coordinates that is an order of magnitude faster then finite difference methods defined on uniform polar grids. This significant decrease in computational complexity is made possible by eliminating the clustering of grid nodes that occurs in uniform polar grids; which, in turn, increases the distance between temporal steps by an order of magnitude.

Proof that the error associated with this numerical scheme decreases quadratically quickly as the distance between grid nodes decreases is supplied in section 2.3. Numerical

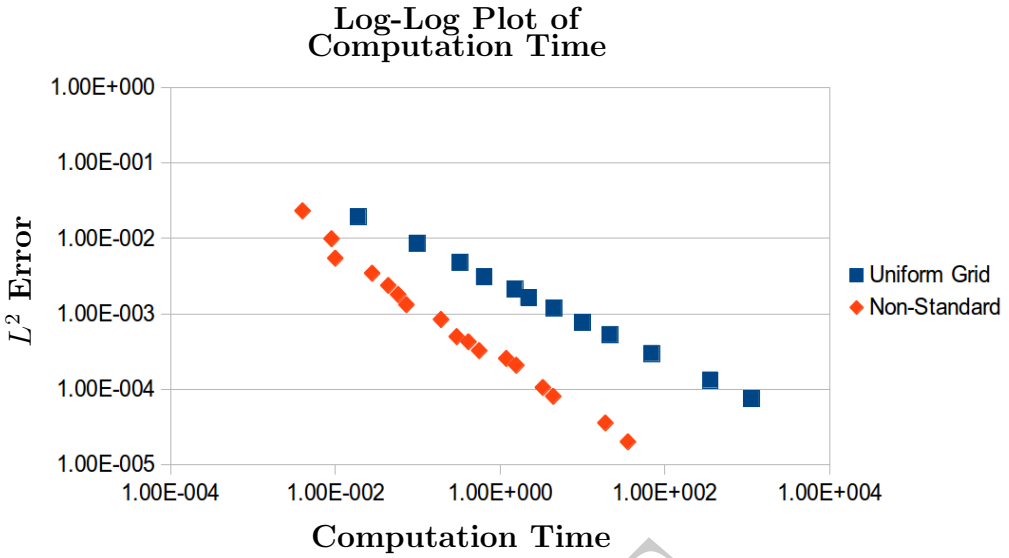

Figure 7. Log-Log plot with relative L^2 error as the vertical axis and computation time as the horizontal axis.

experimentation suggests that this numerical scheme is stable and capable of computing accurate solutions to the wave equation significantly faster then finite difference schemes defined on uniform polar grids. Figures 6 and 7 suggest that this method is capable of producing computations on the same level of accuracy as a uniform polar grid at a fraction of the computational cost.

CITED LITERATURE

[1] G Constantinescu and S. K. Lele. A highly accurate technique for the treatment of flow equations at the polar axis in cylindrical coordinates using series expansions. *Journal of Computational Physics*, 183:165–186, 2002.

[2] M Fox-Rabinovitz, G Stenchikov, M Suarez, and L Takacs. A finite-difference gcm dynamical core with a variable-resolution stretched grid. *Monthly Weather Review*, 125:2943–2968, 1997.

[3] K Fukagata and N Kasagi. Highly energy-conservative finite difference method for the cylindrical coordinate system. *Journal of Computational Physics*, 181:478–498, 2002.

[4] H Grün, G Paltauf, M Haltmeier, and P Burgholzer. Photoacoustic tomography using a fiber based fabry-perot interferometer as an integrating line detector and image reconstruction by model-based time reversal method. *Proc. of SPIE-OSA Biomedical Optics*, 6631, 2007.

[5] Kreiss H.O. and Petersson N.A. A second order accurate embedded boundary method for the wave equation with dirichlet data. *SIAM J. Sci. Computation*, 27:1141–1167, 2006.

[6] Kreiss H.O., Petersson N.A., and Ystrom J. Difference approximations for the second order wave equation. *SIAM J. Numer. Anal.*, 40:1940–1967, 2002.

[7] M Hortal and A Simmons. Use of reduced gaussian grids in spectral models. *Monthly Weather Review*, 1991.

[8] Y. Hristova, P. Kuchment, and L. Nguyen. On reconstruction and time reversal in thermoacoustic tomography in homogeneous and non-homogeneous acoustic media. *Inverse Problems*, 24, 2008.

[9] K Mohseni and T Colonius. Numerical treatment of polar coordinate singularities. *Journal of Computational Physics*, 157:787–795, 2000.

[10] R Shukla and X Zhong. Derivation of high-order compact finite difference schemes for non-uniform grid using polynomial interpolation. *Journal of Computational Physics*, 204:404–429, 2005.

[11] D Surcel and R Laprise. A general filter for stretched-grid models: Application in two dimension polar geometry. *Monthly Weather Review*, 2012.

[12] R Verzicco and P Orlandi. A finite-difference scheme for three-dimensional incompressible flows in cylindrical coordinates. *Journal of Computational Physics*, 123:402–414, 1996.

[13] D Williamson and G Browning. Comparison of grids and difference approximations for numerical weather prediction over a sphere. *Journal of Applied Meteorology*, 12, 1973.

[14] D Williamson and J Rosinski. Accuracy of reduced-grid calculations. *Quarterly Journal of the Royal Meteorological Society*, 126:1619–1640, 2000.

[15] Minghua Xu and Lihong V. Wang. Time reversal and its application to tomography with diffracting sources. *Phys. Rev. Lett.*, 92:3–6, 2004.